

Structural damage localization using spatial wavelet packet signature

C. C. Chang[†] and Z. Sun[‡]

*Department of Civil Engineering, Hong Kong University of Science and Technology,
Clear Water Bay, Kowloon, Hong Kong*

(Received March 27, 2004, Accepted December 8, 2004)

Abstract. In this study, a wavelet packet based method is proposed for identifying damage occurrence and damage location for beam-like structures. This method assumes that the displacement or the acceleration response time histories at various locations along a beam-like structure both before and after damage are available for damage assessment. These responses are processed through a proper level of wavelet packet decomposition. The wavelet packet signature (WPS) that consists of wavelet packet component signal energies is calculated. The change of the WPS curvature between the baseline state and the current state is then used to identify the locations of possible damage in the structure. Two numerical studies, one on a 15-storey shear-beam building frame and another on a simply-supported steel beam, and an experimental study on a simply-supported reinforced concrete beam are performed to validate the proposed method. Results show the WPS curvature change can be used to locate both single and sparsely-distributed multiple damages that exist in the structure. Also the accuracy of assessment does not seem to be affected by the presence of 20-15dB measurement noise. One advantage of the proposed method is that it does not require any mathematical model for the structure being monitored and hence can potentially be used for practical application.

Keywords: damage location; wavelet packet decomposition; model-free method.

1. Introduction

Vibration-based structural condition assessment techniques have been widely studied as a diagnostic tool to detect, locate and quantify structural damage that might occur during structure service period. The basic premise of these techniques is that the damage could alter the physical properties of a structural system and lead to change in its dynamic properties. The measured structural dynamic response could capture these changes and be used for damage assessment. Damage assessment methods can be classified into two categories: model-dependent methods and model-free methods. Theoretically speaking, reliable analytical models can provide more detailed description on structural behavior and thus the model-dependent methods have a better performance on detecting, locating and quantifying damage. Unfortunately, it is generally agreed that accurate analytical models are difficult to obtain, hence these model-dependent methods could be difficult to implement in practice.

[†]Associate Professor, E-mail: cechang@ust.hk

[‡]Post-Doctoral Research Fellow, Corresponding Author, E-mail: cesz@ust.hk

A general procedure for the model-free methods is to directly examine the difference between pre-defined damage indices measured at the current state and some baseline indices measured at some previous state. These damage indices are extracted from the measured response and are supposed to be more sensitive to damage. When the difference exceeds a preset threshold, the presence of damage is indicated. To locate structural damage, multiple sensors are generally required to evaluate the effect of damage on the responses measured at different location of the structure. Pandey, *et al.* (1991) proposed to locate structural damage using the curvature of measured displacement mode shapes. As the curvature was inversely proportional to the flexural stiffness, a reduction of stiffness would lead to a change in the curvature. The change of mode shape curvature could then be used to indicate damage location. Zimmerman and Kaouk (1994) developed a damage detection method based on the changes in dynamically measured stiffness matrix. Pandey and Biswas (1994) proposed to evaluate the change of structural flexibility matrix for detecting both damage presence and damage location. One special advantage of this method was that the flexibility matrix could be easily and accurately estimated from a few lower modes which could be easily obtained from measurement. Stubbs, *et al.* (1995) developed a damage index method for locating damage. Giving the mode shapes before and after damage, a damage index was developed based on the change in strain energy stored in the structure. A statistical method was then used to examine the change in the damage index and then associate these changes to possible damage locations. Zhang and Aktan (1995) stated that the sum of all columns in the flexibility matrix represented the deformed shape of a structure under a unit uniform load. The curvature of the deformed shape could be used to locate damage. Farrar and Jauregui (1998a, b) conducted a comparative experimental study on the I-40 Bridge using the five damage identification algorithms mentioned above. Four damage scenarios, ranging from a two-foot cut at the center of the web to a complete cut to the lower half of the girder, were introduced to simulate fatigue cracks observed in the plate-girder bridges. Some valuable conclusions were made from this important study: (1) standard modal properties such as natural frequencies and mode shapes were poor indicators of damage and (2) more sophisticated methods such as the damage index method (which was based on the second derivatives of mode shapes) and the mode shape curvature method showed an improved capability to detect and locate damage. In addition to these modal-based methods, Sampaio, *et al.* (1999) and Ratcliffe (2000) proposed some methods that were based on the frequency response function (FRF) for damage location. They concluded that the broadband FRF curvature, both near and away from the resonance, offered improved accuracy when compared to the modal-based approach. Numerical and experimental studies verified that the broadband FRF based methods were very suitable for practical application due to its simplicity and model-free nature.

Recently, Sun and Chang (2002) proposed a structural condition index termed as the wavelet packet signature (WPS). This index consisted of component signal energies obtained from performing wavelet packet decomposition on the measured response. Results showed that this WPS was sensitive to the change of structural properties and yet insensitive to the measurement noise. When combined with a well-trained neural network (NN) model, the change of the measured WPS from a single sensor could be used to detect, locate and quantify structural damage. The success of this approach however depends highly on the accuracy of the NN model. The approach can be classified as a model-dependent method as the training of this NN model requires detailed mathematical information for the structure under both healthy and damaged condition.

In this study, a model-free method based on the WPS curvature is proposed for locating damage in beam-like structures. Two numerical studies, one on a 15-storey shear-beam building frame and another on a simply-supported steel beam, are performed to validate the proposed method. Both single and

multiple-damage scenarios are studied. The effect of measurement noise on the accuracy of damage assessment is analyzed and discussed. Furthermore, an experimental study on a simply-supported reinforced concrete beam is performed to verify the practical applicability of the method.

2. Formulation

2.1. Wavelet packet signature (WPS)

Wavelet packets, $\psi_{j,k}^i(t)$, are time functions that relate to the normal wavelet functions $\psi^i(t)$ through,

$$\psi_{j,k}^i(t) = 2^{j/2} \psi^i(2^j t - k) \quad i = 1, 2, \dots \quad (1)$$

where the integers i, j and k are the modulation, the scale and the translation parameter, respectively. The wavelets functions ψ^i are obtained from the following recursive relationships,

$$\psi^{2i}(t) = \sqrt{2} \sum_k h(k) \psi^i(2t - k) \quad (2)$$

$$\psi^{2i+1}(t) = \sqrt{2} \sum_k g(k) \psi^i(2t - k) \quad (3)$$

Note that the first two wavelets are the so-called scaling function $\varphi(t)$ and mother wavelet function $\psi(t)$,

$$\psi^0(t) = \varphi(t), \quad \psi^1(t) = \psi(t) \quad (4a, b)$$

The discrete filters $h(k)$ and $g(k)$ are the quadrature mirror filters associated with the scaling function and the mother wavelet function. Any measurable and square-integrable function $s(t)$ can be decomposed into wavelet packet component functions $s_j^i(t)$,

$$s(t) = \sum_{j=1}^{2^i} s_j^i(t) \quad (5)$$

The decomposition process is a recursive filter-decimation operation (Coifman and Wickerhauser 1992). The decomposed wavelet packet component signal $s_j^i(t)$ can be expressed as a linear combination of wavelet packet functions $\psi_{j,k}^i(t)$,

$$s_j^i(t) = \sum_k c_{j,k}^i \psi_{j,k}^i(t) \quad (6)$$

The wavelet packet coefficients $c_{j,k}^i$ can be obtained from,

$$c_{j,k}^i = \int_{-\infty}^{\infty} s(t) \psi_{j,k}^i(t) dt \quad (7)$$

Each component in the wavelet packet decomposition (WPD) tree can be viewed as the output of a filter tuned to a particular basis function, thus the whole tree can be regarded as a filter bank. At the

top of the WPD tree (lower decomposition level), the WPD yields a good resolution in the time domain but a poor resolution in the frequency domain. On the other hand, at the bottom of the WPD tree (higher decomposition level), the WPD results in a good resolution in the frequency domain yet a poor resolution in the time domain. For the purpose of structural health monitoring, frequency domain information tends to be more important and thus a high level of the WPD is often required to detect the minute changes in the signals.

After the WPD, the problem then is how these decomposed signals can be used for structural condition assessment. Sun and Chang (2002) demonstrated numerically using a three-span bridge that the wavelet packet component energies were sensitive parameters and could be used as a structural condition signature. These component energies are defined as,

$$E_j^i = \int_{-\infty}^{\infty} s_j^i(t)^2 dt \quad (8)$$

where E_j^i is the i -th wavelet packet component energy at the j -th level of decomposition. It can be shown that, when the mother wavelet is semi-orthogonal or orthogonal, the signal energy E_s is the summation of the j -th level component energies as follows:

$$E_s = \int_{-\infty}^{\infty} s^2(t) dt = \sum_j E_j^i \quad (9)$$

After j levels of decomposition, a total of 2^j component functions, that come with an equal bandwidth of $f_N/2^j$ where f_N is the Nyquist frequency, can be obtained. Arranging these component functions in an ascending frequency order, the central frequency of the i -th component function, f_i , can be expressed as

$$f_i = \frac{(2i-1)f_N}{2^{j+1}} \quad (10)$$

2.2. Spatial WPS curvature

To obtain the spatial WPS vibration shape, a set of WPS's are first extracted from the structural response (displacement, velocity or acceleration) measured from the distributed sensor locations. For better comparison, this spatial WPS vibration shape is firstly normalized as follows,

$$\bar{E}_j^i(n) = \frac{E_j^i(n)}{\max(E_j^i)} \quad (11)$$

where $E_j^i(n)$ and $\bar{E}_j^i(n)$ are the i -th wavelet packet component energy of the j -th level decomposition at location n before and after normalization, respectively. The curvature of the WPS vibration shape at location n , $\bar{E}_j^i(n)''$, can be estimated by the three-point approximation. To estimate the spatial WPS curvature at sensor n which is not at the boundary, the WPSs measured from sensors $n-1$, n , and $n+1$ are required for the following central difference approximation,

$$\bar{E}_j^i(n)'' = \frac{\bar{E}_j^i(n+1) - 2\bar{E}_j^i(n) + \bar{E}_j^i(n-1)}{\Delta x^2} \quad (12)$$

where Δx is the constant spatial distant between two adjacent sensors. At the boundaries of the structure, the curvatures of the WPS vibration shape are estimated by either backward or forward

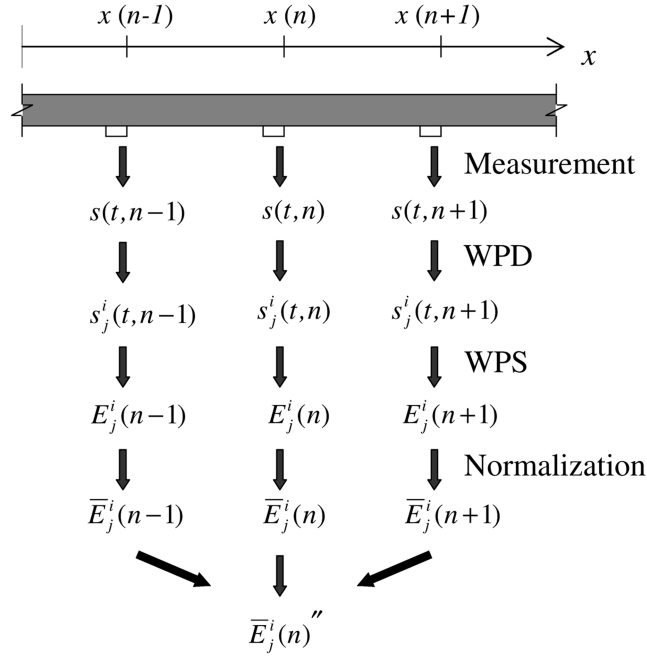


Fig. 1 Computation of spatial WPS curvature

difference approximation. If the sensors are unevenly distributed in the spatial domain, the curvature of the WPS vibration shape at location n can be estimated as follows.

$$\bar{E}_j^i(n)'' = \left(\frac{\bar{E}_j^i(n+1) - \bar{E}_j^i(n)}{x(n+1) - x(n)} - \frac{\bar{E}_j^i(n) - \bar{E}_j^i(n-1)}{x(n) - x(n-1)} \right) \bigg/ \left(\frac{x(n+1) - x(n-1)}{2} \right) \quad (13)$$

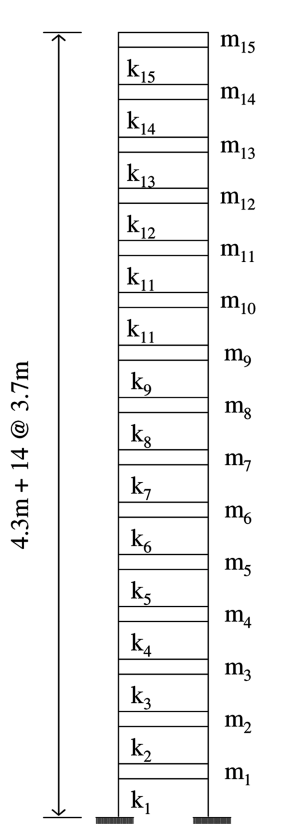
where $x(n)$ is the spatial coordinate of the n -th sensors. Similar to the use of mode shape curvature, this WPS vibration shape curvature can be used to indicate the location of damage for beam-like structures. Fig. 1 outlines the procedure to compute the spatial WPS vibration shape curvature.

3. Case studies

To demonstrate and verify the proposed spatial WPS method, two numerical examples and one experimental study are performed. In these three case studies, the mother wavelet is assumed to be the 15-th wavelet function in the Daubechies wavelet family (Daubechies 1992).

3.1. Case 1: Numerical study on a 15-storey shear-beam building frame

A 15-storey shear-beam building frame with variable stiffness and mass coefficients is shown in Fig. 2. The height between the ground and the 1st storey is 4.3 m and the rest of the storey heights are constant of 3.7 m. The damping ratios for all modes are assumed to be 2%. Four levels of damage are assumed to occur in the 9th storey and can be modeled by 20, 40, 60 and 80% reduction of stiffness



i	Mass m_i (ton)	Stiffness k_i (10^7N/m)
1	246.4	5.0
2	398.6	5.0
3	393.2	5.0
4	393.2	4.5
5	390.5	4.5
6	390.5	4.5
7	390.5	4.2
8	390.5	4.2
9	390.5	4.0
10	390.5	4.0
11	390.5	4.0
12	390.5	4.0
13	390.5	3.8
14	584.4	3.6
15	362.4	2.8

Fig. 2 A 15-storey shear-beam building frame

coefficient k_9 , respectively. Dynamic simulations are performed on the healthy beam as well as on the four damaged cases. During the simulations, an impact force of 1 kN is applied at the top floor. The simulated acceleration time histories at all 15 stories are decomposed into the 6th level wavelet packet tree. Wavelet packet component signal energies are then calculated and sorted in the ascending frequency order.

Fig. 3 shows the differences of the spatial WPS distribution, the spatial WPS slope, and the spatial WPS curvature for the first two terms between the healthy and the damaged (corresponding to the case of 40% k_9 reduction) states. It is seen that the change of the spatial WPS curvature is much more significant than that of the other two indices. Also the spatial WPS curvature can correctly identify the location of damage between the 8th and the 9th storey. Both the 1st and the 2nd term of the spatial WPS curvature can identify the damage location.

Fig. 4 shows the spatial WPS curvature differences between the healthy frame and the frame with four damage levels. It is seen again that the damage location can be correctly identified by both WPS terms. Also the curvature difference increases as the damage becomes more severe. To check the effect of measurement noise, independent noises were added to the simulated acceleration time histories at all 15 stories before the wavelet packet decomposition. The noises that we added are broadband Gaussian white noises whose intensities are defined by the following signal-to-noise ratio (SNR),

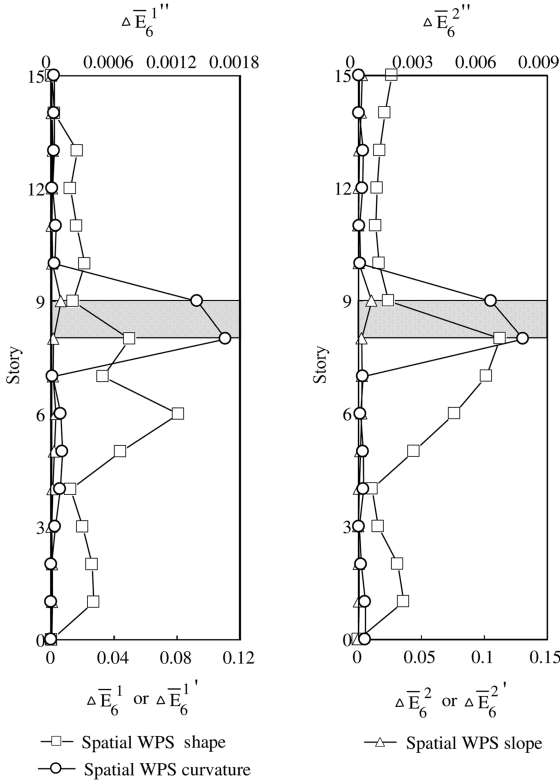


Fig. 3 Changes of WPS spatial distribution, slope and curvature due to 40% reduction on k_9

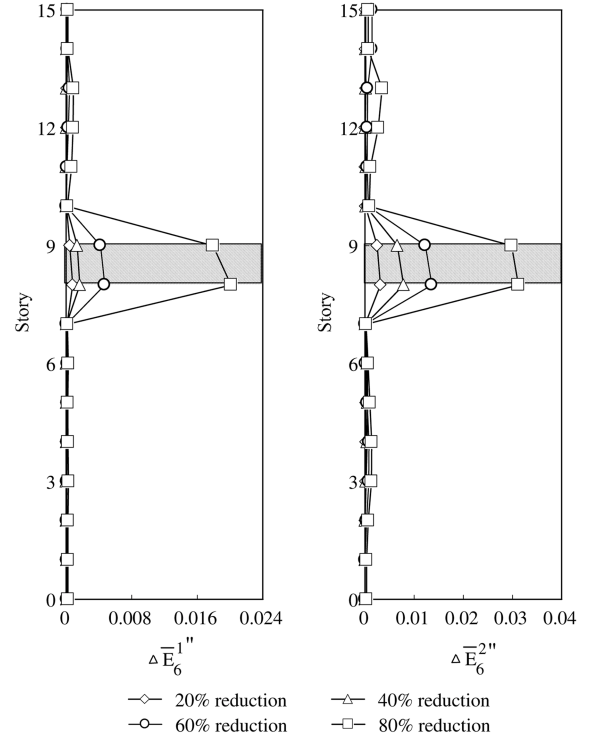


Fig. 4 Spatial WPS curvature differences for four levels of stiffness reduction on k_9

$$\text{SNR} = 20 \log_{10} \frac{A_S}{A_N} \quad (\text{in dB}) \quad (14)$$

where A_S and A_N refer to the root-mean-square (RMS) value of the signal and the noise, respectively. Fig. 5 shows the spatial WPS curvature difference under 40% k_9 reduction and when the responses are contaminated with 30 and 20 dB noise. It is seen that the proposed approach is still able to locate damage under 30 dB measurement noises. However, the WPS curvature difference starts to fluctuate and fail to distinctly identify the damage location when the magnitude of the measurement noise increases to 20 dB. Note the noise effect on damage localization also depends on the damage position and the characteristics of applied load. The noise immunity of the proposed technique is hence case dependent and cannot be affirmatively concluded.

3.2. Case 2: Numerical study on a simply-supported steel beam

Fig. 6(a) shows a simply supported steel beam modeled using 20 beam elements. The material and geometric properties for the beam are: module of elasticity $E = 2.06 \times 10^5 \text{ MPa}$, mass density $\rho = 7800 \text{ kg/m}^3$, cross-sectional area $A = 6 \times 10^{-4} \text{ m}^2$ and moment of inertia $I = 1.8 \times 10^{-9} \text{ m}^4$. The displacement response time histories at all 19 nodes except the two support nodes are assumed to be

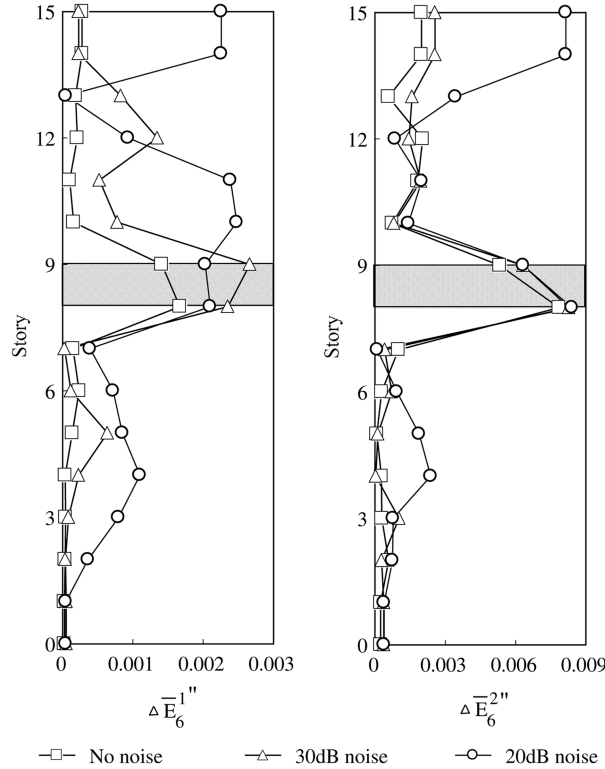


Fig. 5 Spatial WPS curvature differences for 40% k_g reduction under 30 dB and 20 dB measurement noise

available for locating damage. These response time histories are processed through 8 levels of wavelet packet decomposition and the WPS is constructed. Fig. 6(b) shows the normalized spatial WPS curvature of the first four components for the beam without any damage. These WPS distributions will be used as the baseline for calculating the WPS curvature change in the following analyses. A total of 12 damage scenarios as shown in Table 1 are assumed: 4 single-damage scenarios (SD1-SD4), 4 double-damage scenarios (DD1-DD4) and 4 triple-damage scenarios (TD1-TD4). The 4 single-damage scenarios assume that the rigidity of the 10th element is damaged and reduced by 5, 10, 15 and 20%, respectively. The 4 double-damage scenarios assume that the 10th element is damaged and its rigidity is reduced by 10% while the rigidity of the 5th element is reduced by 5, 10, 15 and 20%, respectively. Finally, the damage locations and the damage severities of the 4 triple-damage scenarios are assumed quite arbitrarily as can be seen in Table 1.

Fig. 7 shows the curvature differences of the first 4 terms of the WPS under the 4 single-damage scenarios (SD1-SD4). The results show that the WPS curvature differences between the damaged scenarios and the healthy condition can correctly identify the location of damage that occurs at the 10th element. Also it can be seen from this figure that the curvature difference increases as the severity of damage increases (from SD1 to SD4). This result suggests that the spatial WPS curvature difference has a potential for qualitative assessment of damage severity. To study whether the current method would work under sparse measurement, it is assumed that only the displacement time histories at the odd nodes are measured (a total of 9 displacement time histories). Fig. 8 shows the curvature differences of the first 4 terms of the WPS under the 4 single-damage scenarios (SD1-SD4) calculated

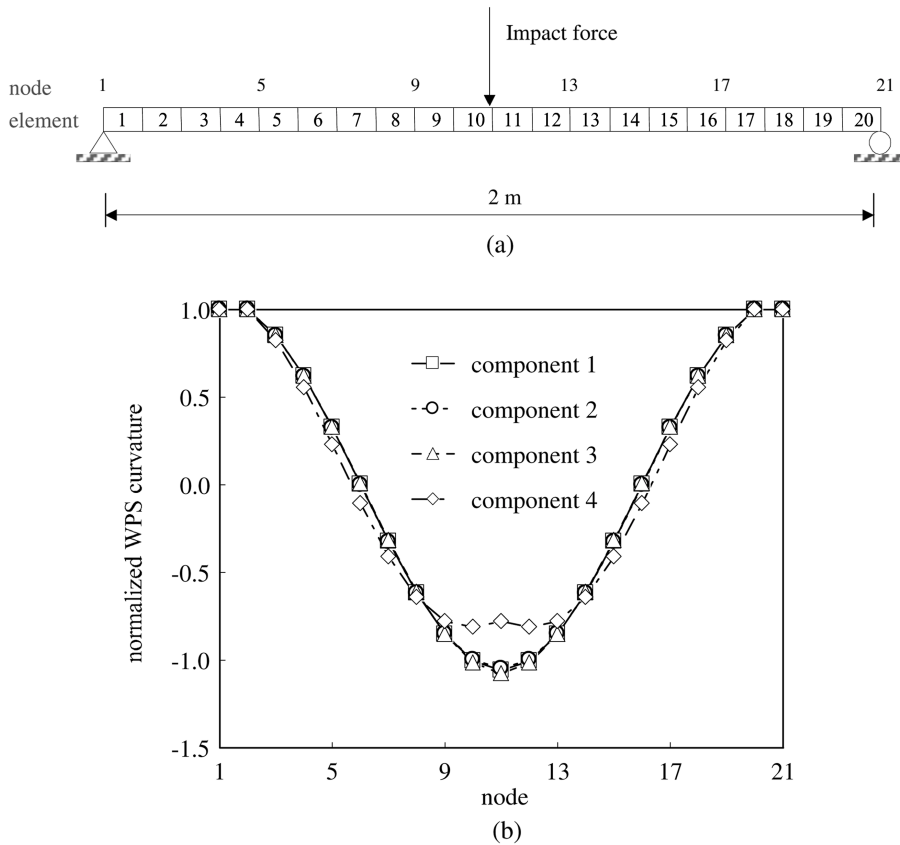


Fig. 6 (a) A simply-supported beam structure modeled using 20 beam elements and (b) the spatial distribution of its first four WPS components

Table 1 Description of damage cases

No.	Damage 1	Damage 2	Damage 3
SD1	EI_{10} : 5%	-	-
SD2	EI_{10} : 10%	-	-
SD3	EI_{10} : 15%	-	-
SD4	EI_{10} : 20%	-	-
DD1	EI_5 : 5%	EI_{10} : 10%	-
DD2	EI_5 : 10%	EI_{10} : 10%	-
DD3	EI_5 : 15%	EI_{10} : 10%	-
DD4	EI_5 : 20%	EI_{10} : 10%	-
TD1	EI_4 : 20%	EI_{12} : 25%	EI_{15} : 15%
TD2	EI_6 : 20%	EI_8 : 10%	EI_{12} : 15%
TD3	EI_4 : 10%	EI_{12} : 25%	EI_{18} : 15%
TD4	EI_7 : 5%	EI_{12} : 25%	EI_{17} : 10%

from these 9 measurements. It is seen that the curvature differences of all 4 terms reach their respective maximums at node 11 under these 4 single-damage scenarios. These results suggest that the WPS

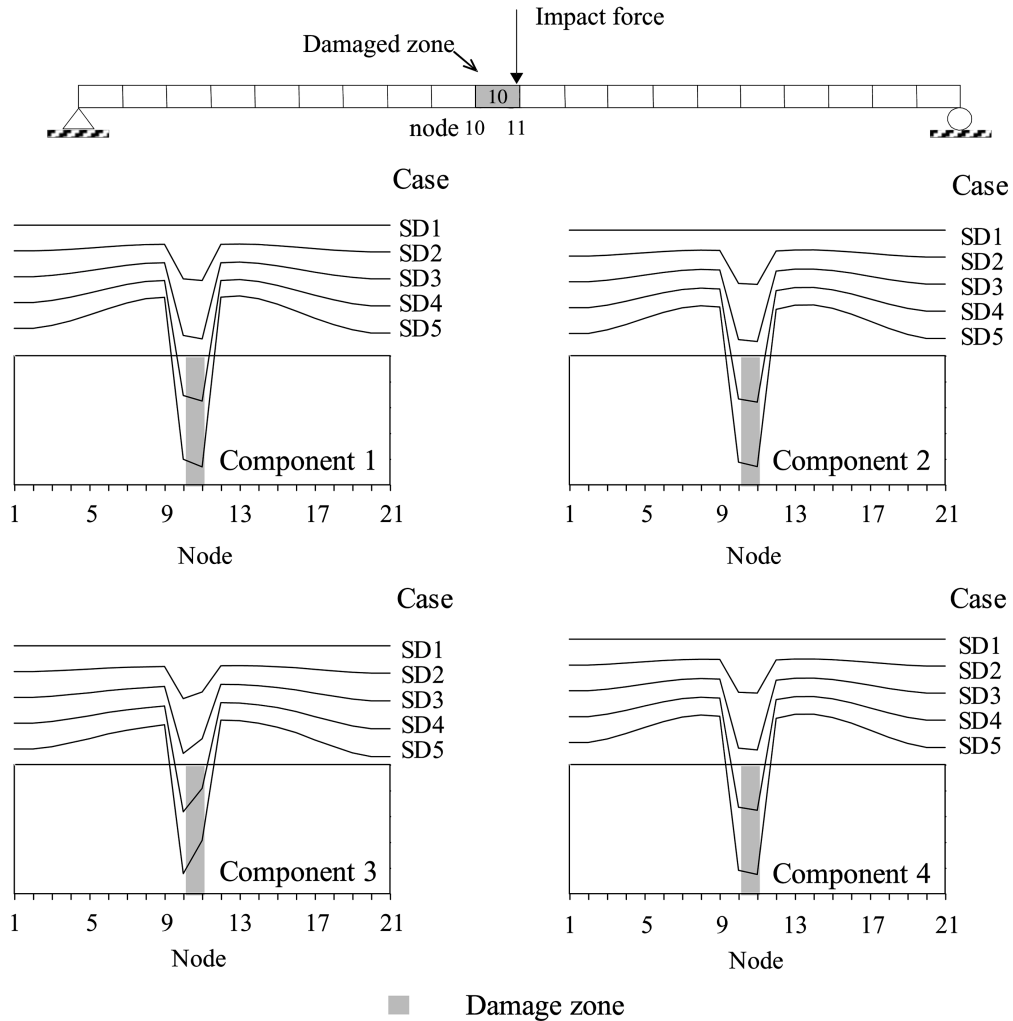


Fig. 7 The spatial WPS curvature differences for different levels of damage in element 10

curvature difference can still give a pretty accurate indication for damage location even though time-history responses at some locations are not available.

Fig. 9 shows the WPS curvature differences of the first 4 terms of the WPS under the 4 double-damage scenarios (DD1-DD4). These 4 damage scenarios are based on the SD2 scenario (the rigidity of the 10th element reduced by 10%) with an additional stiffness reduction of the 5th element by 5, 10, 15 and 20%, respectively. The results show that the curvature differences of the first 4 terms of the WPS all show two peaks that correspond to the 5th and 10th element. This again suggests that the WPS curvature difference is able to locate double damages quite correctly. It is also seen that, just as in the case of single damage, the curvature difference increases as the damage severity increases.

The results for the 4 triple-damage scenarios are plotted in Fig. 10. It is seen that when the damage locations are quite separated and the damage severities are about the same such as for the case of TD1 (rigidity of the 4th, 12th and 15th element reduced by 20, 25 and 15%, respectively), the WPS

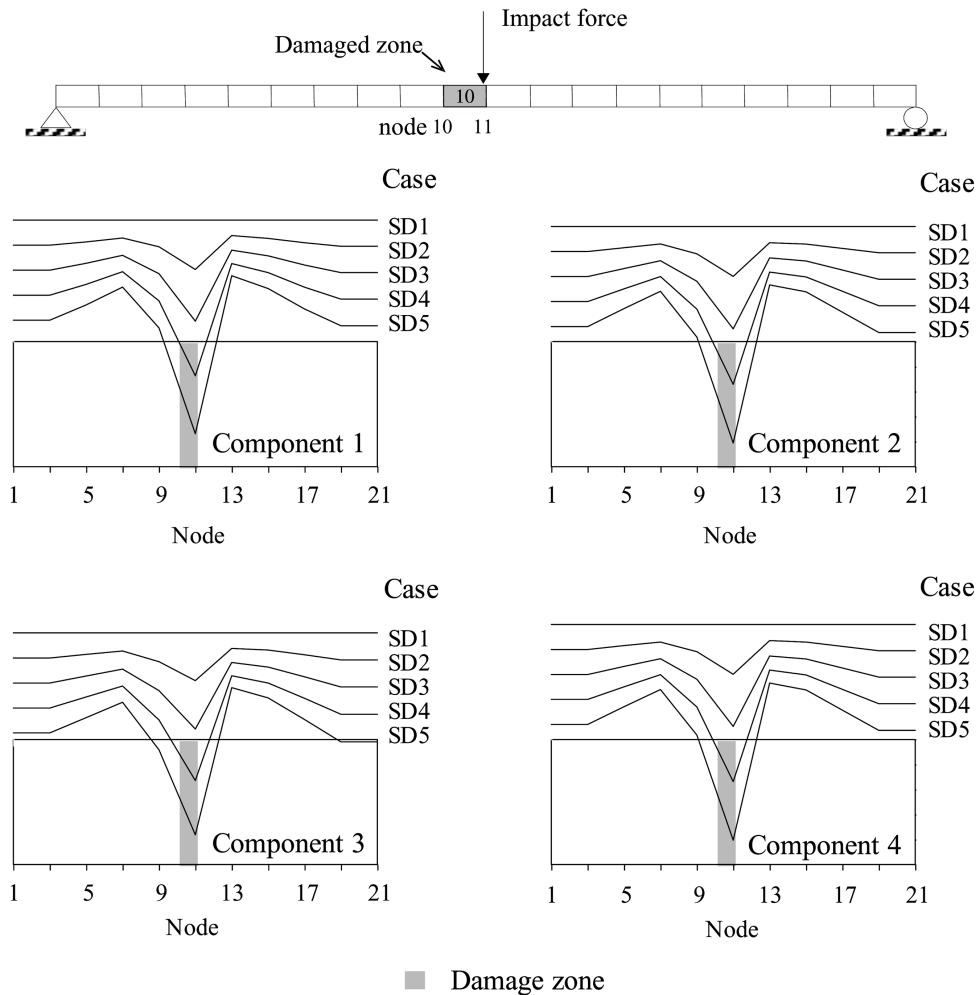


Fig. 8 The spatial WPS curvature differences for different levels of damage in element 10 under sparse installation

curvature difference can correctly and distinctly locate damages. When the damage locations are close such as the case of TD2 (rigidity of the 6th, 8th and 12th element reduced by 20, 10 and 15%, respectively), some damage location might not be clearly identified (damage at the 8th element). Also when the damage severities are not with a similar magnitude, some less severe damages might not be located distinctly, such as the damage of the 4th element for TD3 and the damage of the 7th element for TD4.

To study the effect of measurement noise, independent broadband white noises with magnitudes of 20, 15, 10 and 5 dB were added to the simulated displacement time histories at all 15 stories before the wavelet packet decomposition. Fig. 11 shows the curvature differences of the first 4 terms of the WPS for the single-damage scenario SD2 (rigidity of the 10th element reduced by 10%) with these measurement noises added. The results show that the proposed technique is able to correctly identify the damage location even with 10dB noises added to the responses for this case.

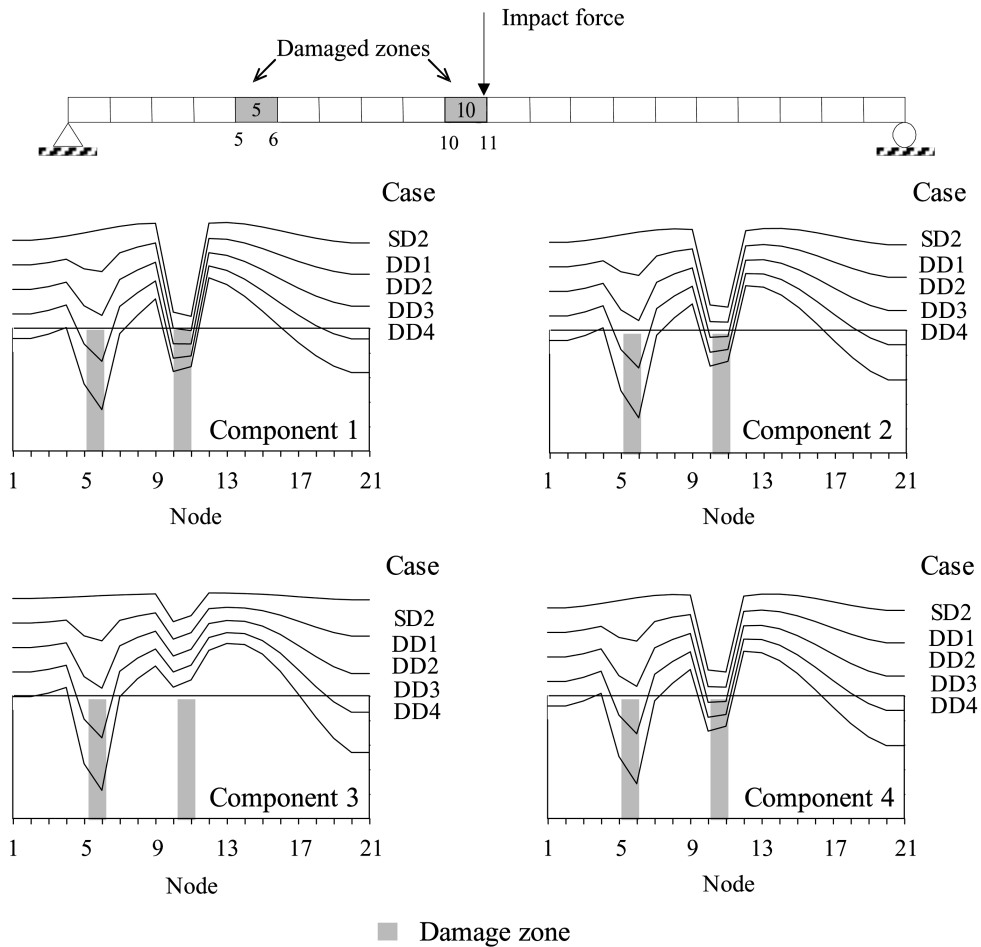


Fig. 9 The spatial WPS curvature differences for the double-damage cases DD1-DD4

3.3. Case 3: Experimental study on a simply-supported RC beam

To further verify the applicability and the accuracy of the WPD-based damage localization technique, an experimental study on a simply supported RC beam was conducted. The RC beam came with a length of 5 m and was placed on two roller supports to emulate simply supported boundary condition. The span length between the two supports was 4.8 m. The cross section of the beam was 0.25 m deep and 0.2 m wide. The tension reinforcements consisted of 2 high strength steel bars with a diameter of 20-mm (2T20) and the hanger bars were 2 mild steel bars of 10-mm diameter. Mild steel of 10-mm-diameter was used to make 35 stirrups for the beam. Detailed dimensions of the beam are shown in Fig. 12.

To damage the beam, a static load with four sequentially increasing magnitudes, from 12 kN to 24 kN with an increment of 4 kN, was applied at the mid-span of the beam as shown in Fig. 13(a). These 4 load conditions were designated as states S1 to S4. As a comparison, the undamaged state of the beam was denoted as S0. Impact forces produced by an impact hammer were applied at three separate locations (points A, B and C) on the top surface of the beam before application of the static load (S0) and after

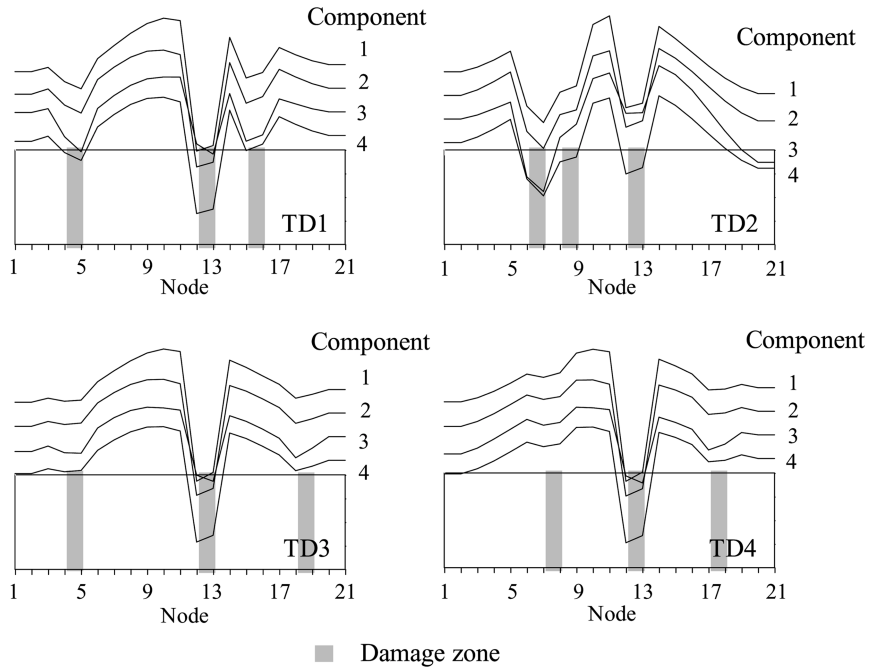


Fig. 10 The spatial WPS curvature differences for the triple-damage cases TD1-TD4

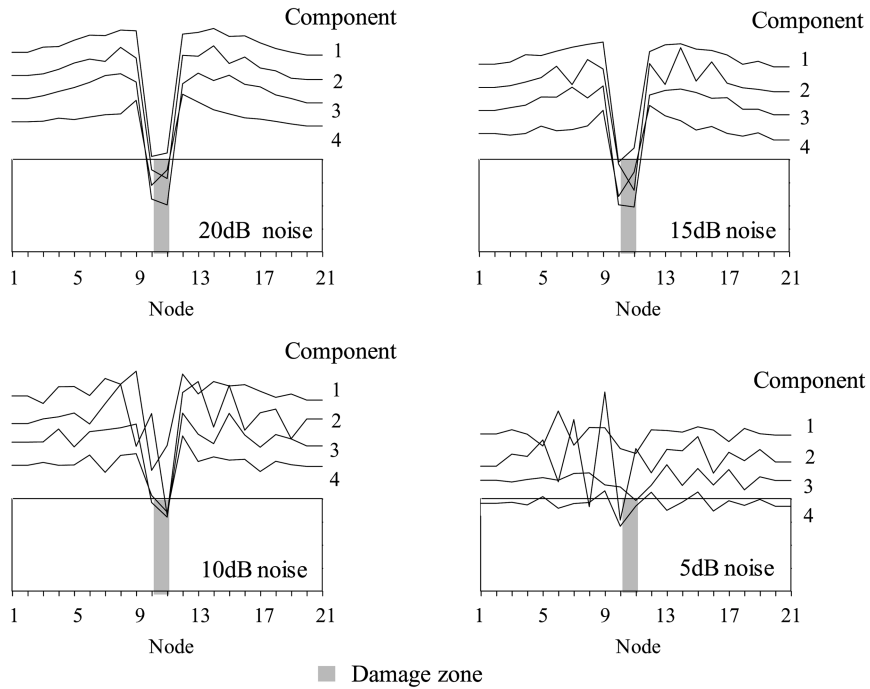


Fig. 11 The spatial WPS curvature difference for 10% *EI* reduction of element 10 with different levels of measurement noise

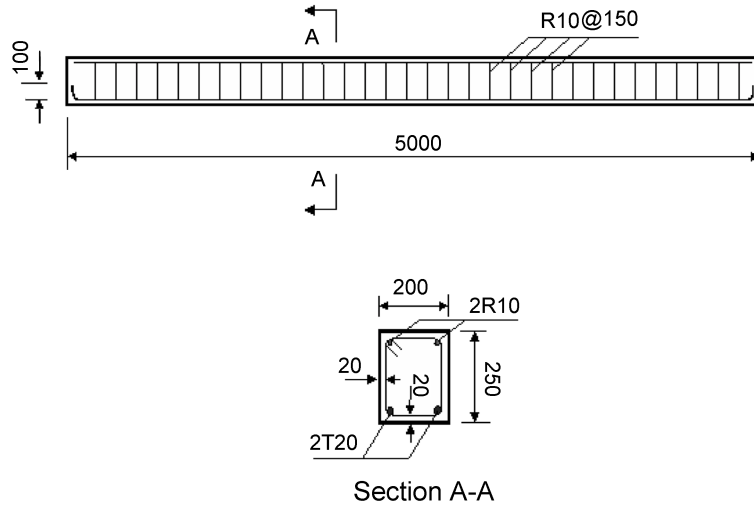


Fig. 12 Details of the RC beam (unit: mm)

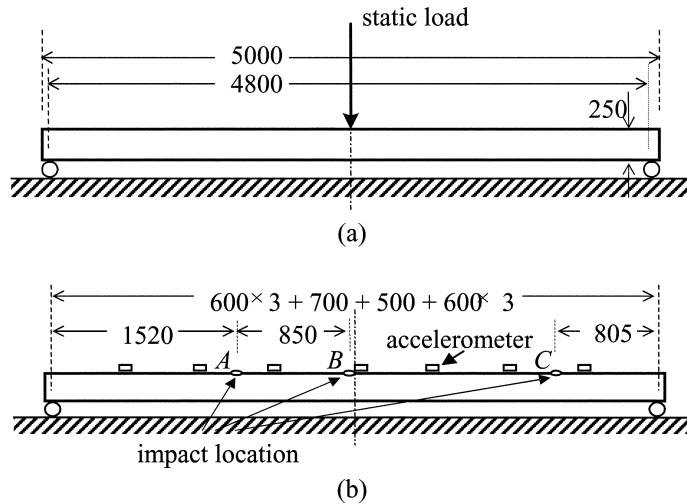


Fig. 13 (a) Experimental setup for static loading tests and (b) impact tests (unit: mm)

each application of the static load (S1 through S4). A total of 7 accelerometers were installed on the top surface of the beam with locations indicated in Fig. 13(b). A signal conditioning system, which has a 66-dB gain for signal below 50 Hz, is used for gain adjustment and filtering. The sampling frequency was set at 200 Hz.

Fig. 14 shows the cracks developed at the lower surface of the beam after the application of the static load. It is seen that the cracks were initiated near the mid-span of the beam where the maximum tensile stress occurred. Under the current experimental set-up, it is apparent that the mid-span region is the most possible location for damage occurrence if there is any.

Seven sets of acceleration records from each test were measured and decomposed using the 8th level WPD and spatial WPS curvatures were then obtained. The changes of the first 4 terms of the WPS

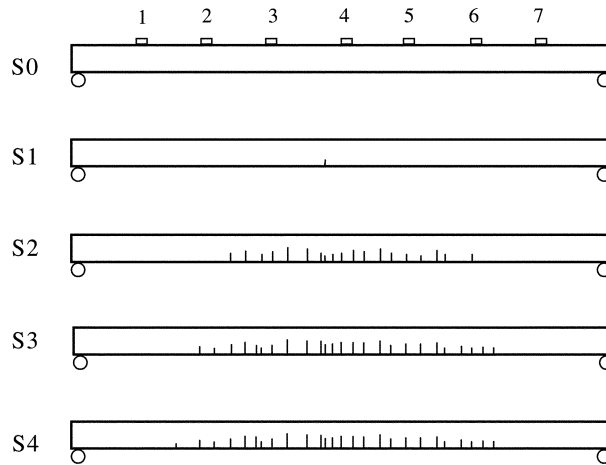


Fig. 14 Observed cracks under damage states S1-S4

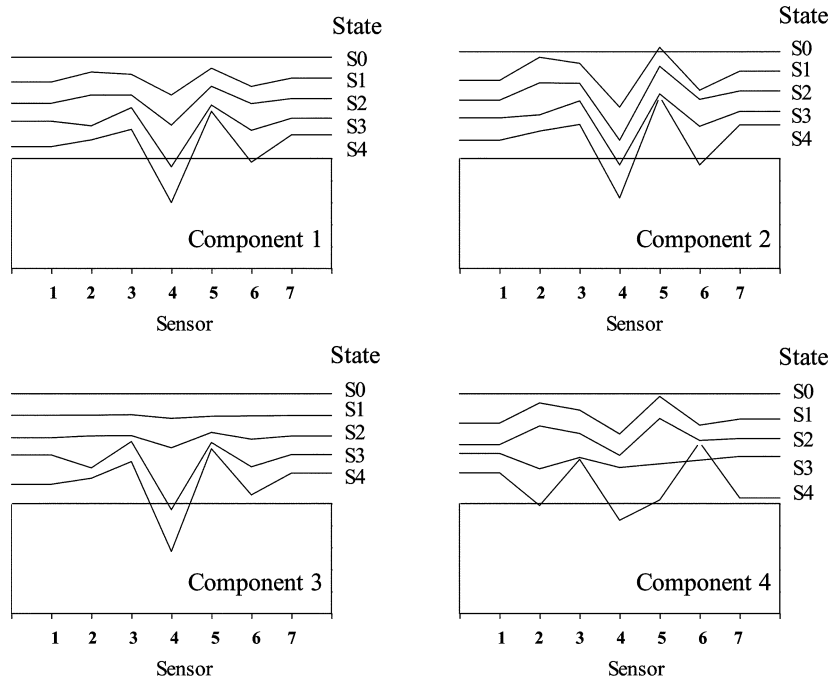


Fig. 15 The spatial WPS curvature differences between the damage states S1-S4 and the baseline state S0 (impact at A)

curvature between the baseline state (S0) and the damage states (S1-S4) are plotted in Fig. 15 which corresponds to applying the impact force at A. It is seen from this figure that the WPS curvature differences reach their maximums at the mid-span of the beam for the first 3 components for all 4 damage states. These results suggest that there is a potential damage occurring around the mid-span of the beam. It is also seen that the maximum of the curvature difference increases as the magnitude of static load increases. This increasing trend echoes the phenomenon observed from the previous two

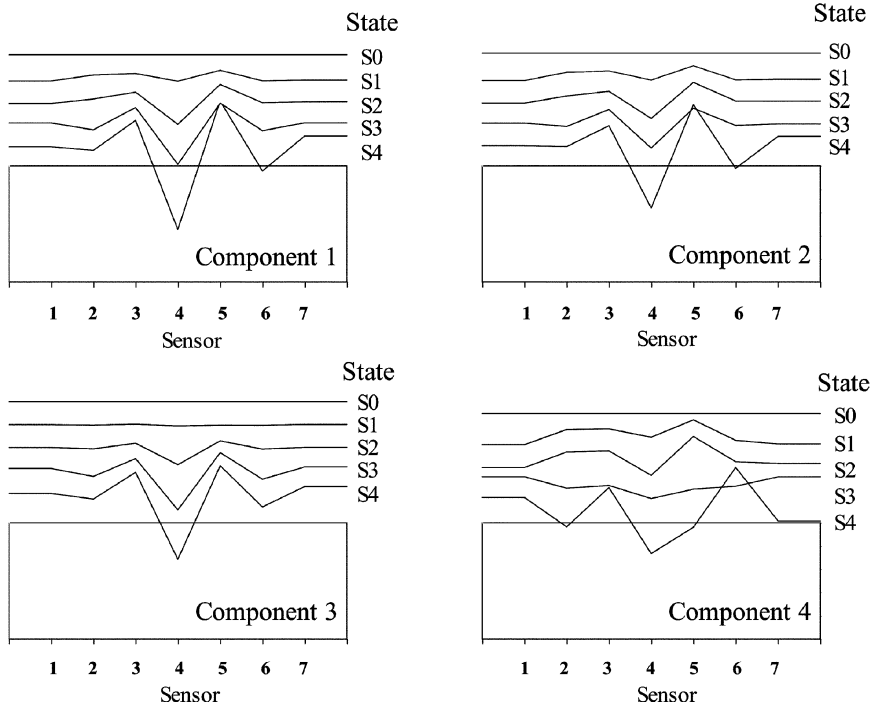


Fig. 16 The spatial WPS curvature difference between the damage states S1-S4 and the baseline state S0 (impact at B)

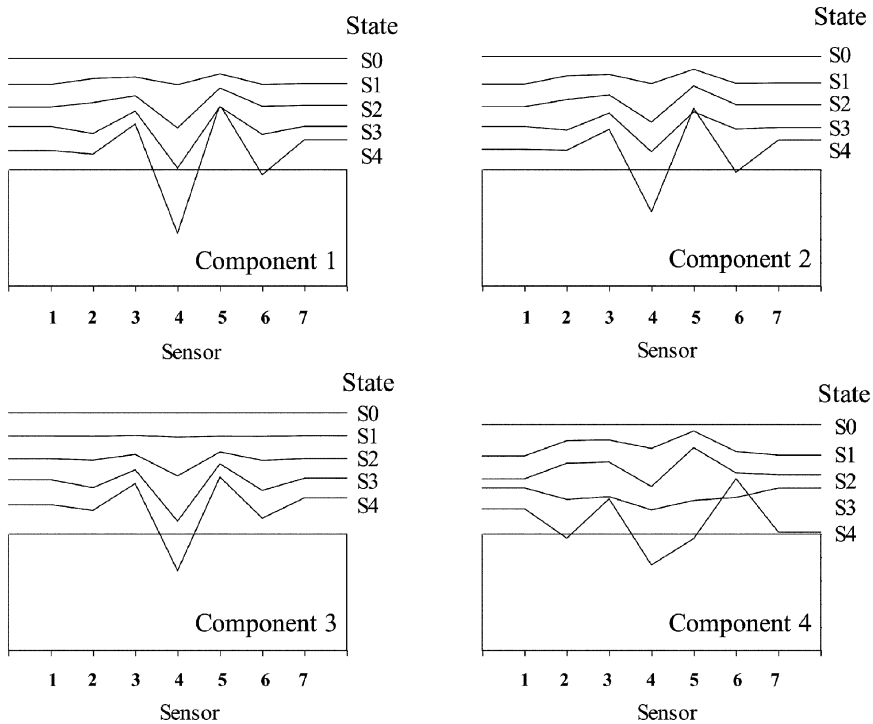


Fig. 17 The spatial WPS curvature differences between damage states S1-S4 and the baseline state S0 (impact at C)

numerical cases. Similar results can be seen from Figs. 16 and 17 which correspond to applying the impact force at point B and C, respectively. This experimental study suggests that the proposed spatial WPS curvature method can be used to locate possible damage in the beam. Also the location of impact force does not seem to affect the diagnostic result.

4. Concluding remarks

In this study, a wavelet packet based method is proposed for the level two damage assessment, including damage occurrence and damage location, for beam-like structures. The proposed technique is a model-free method that does not require any mathematical information about the structure being monitored. This method requires that the displacement or the acceleration response time histories at various locations along a beam-like structure both before and after damage be available for damage assessment. These responses are processed through a proper level of wavelet packet decomposition and the wavelet packet signature (WPS) that consists of wavelet packet component signal energies is calculated. The change of the WPS curvature between the baseline state and the current state is then used to identify the locations of possible damages in the structure.

Two numerical examples involving one shear-beam building frame and one simply-supported steel beam and one experimental study on a simply-supported RC beam are studied to validate the proposed method. Based on the results obtained, it can be concluded that the WPS curvature change can be used to locate damages that might have occurred in the structure. This WPS curvature change appears to increase as the damage becomes more severe. Locating multiple damages is also possible as long as the damages are not closely spaced and their severities are not drastically different. The accuracy of assessment does not seem to be significantly affected by the presence of measurement noise. In the numerical examples, the damage location can still be correctly identified even when some broadband noises are added to the simulated responses. Finally, it is found from the experimental study that the location of excitation does not affect the assessment results. As a model-free method, the proposed technique shows a potential to be used for practical application.

Acknowledgements

This study is supported by the Hong Kong Research Grants Council Competitive Earmarked Research Grant HKUST6030/02E. The authors wish to thank Mr. C.K. Wong, S.C. Wong and K.C. Tse for the experimental study that they have undertaken as a part of their undergraduate final year project.

References

- Coifman, R. R. and Wickerhauser, M. V. (1992), "Entropy-based algorithms for best basis selection", *IEEE Trans. Information Theory*, **38**, 713-718.
- Daubechies, I. (1992), *Ten Lectures on Wavelets*, CBS-NSF Regional Conferences in Applied Mathematics.
- Farrar, C. R. and Jauregui, D. A. (1998a), "Comparative study of damage identification algorithms applied to a bridge: I. Experiment", *Smart Materials and Structures*, **7**, 704-719.
- Farrar, C. R. and Jauregui, D. A. (1998b), "Comparative study of damage identification algorithms applied to a bridge: II. Numerical study", *Smart Materials and Structures*, **7**, 720-731.

- Pandey, A. K., Biswas, M. and Samman, M. M. (1991), "Damage detection from changes in curvature mode shapes", *J. Sound Vib.*, **145**, 321-332.
- Pandey, A. K., Biswas, M. (1994), "Damage detection in structures using changes in flexibility", *J. Sound and Vib.*, **145**, 321-332.
- Ratcliffe, C. R. (2000), "A frequency and curvature based experimental method for locating damage in structures", *J. Vib. Acoust.*, **122**, 324-329.
- Sampaio, R. P. C., Maia, N. M. M. and Silva, J. M. M. (1999), "Damage detection using the frequency-response-function curvature method", *J. Sound Vib.*, **226**(5), 1029-1042.
- Stubbs, N., Kim, J. T. and Farrar, C. R. (1995), "Field verification of a nondestructive damage localization and severity estimation algorithm", *Proceedings of 13th Int. Modal Analysis Conference*, 210-218.
- Sun, Z. and Chang, C. C., (2002), "Structural damage assessment based on wavelet packet transform", *J. Struct. Eng.*, ASCE, **128**(10), 1354-1361.
- Zhang, Z. and Aktan, A. E. (1995), "The damage indices for the constructed facilities", *Proceedings of 13th Int. Modal Analysis Conference*, **12**, 1520-1529.
- Zimmerman, D. C. and Kaouk, M. (1994), "Structural damage detection using a minimum rank update theory", *J. Vib. Acoust.*, **116**, 222-230.

CC